ELSEVIER

Nuclear Engineering and Design 177 (1997) 285–301

Nuclear Engineering and Design

The mixing of particle clouds plunging into water

S. Angelini, T.G. Theofanous *, W.W. Yuen

Center for Risk Studies and Safety, Departments of Chemical and Mechanical Engineering, University of California, Santa Barbara, CA 93106, USA

Abstract

This work addresses certain fundamental aspects of the premixing phase of steam explosions. At issue are the multifield interaction aspects under highly transient, multidimensional conditions and in the presence of strong phase changes. They are addressed in an experiment (the MAGICO-2000) involving well-characterized particle clouds mixing with water and detailed measurements on both external and internal characteristics of the mixing zone. Both cold and hot (up to 1500°C) particle clouds are considered in conjunction with saturated and subcooled water pools. The PM-ALPHA code is used as an aid in interpreting the experimental results and the exercise reveals good predictive capabilities for it. © 1997 Elsevier Science S.A.

1. Introduction

This paper describes certain fundamentally-oriented experiments with particle clouds plunging into water. Of special interest are the dynamics of the (transient) interaction, the multidimensional behavior and, in the case of hot particles, phase-change phenomena and the resulting void fractions in the mixing region. While in a broad sense the subject could be classified under the well-established field of 'fluidization', it is, for the most part, outside the main realms investigated previously. That this is so is not immediately obvious, but it will be demonstrated by the results of the present work.

Our present interest derives from the study of steam explosions. It is known that such explosions propagate through coarse-scale mixtures (the 'premixtures') of a 'hot' liquid (usually a melt) into a coolant (typically water). In the metastable state of a premixture the hot liquid is surrounded by vapor blankets (film boiling) and depending on the particulars of the interaction (size of mixing zone, temperature of melt, coolant subcooling, etc.) it may contain more or less voids (that is, vapor as the third component). It is now possible to compute this propagation and the resulting shock pressures to the surrounding structures (Theofanous and Yuen, 1994) provided the spatial distributions of the premixture constituents are known at the instant that an explosion is triggered. Thus, the study of 'premixing' as a phenomenon provides the key link between the independent variables that characterize a melt-pour scenario (i.e. pour geometry, quantities, water pool geometry and subcooling) and the resulting explosion itself.

* Corresponding author. Present address: Center for Risk Studies and Safety, 6740 Cortona Drive, Goleta, CA 93117, USA. Tel.: +1 805 8934900; fax: +1 805 8934927; e-mail: sergio@engineering.ucsb.edu

PII S0029-5493(97)00200-8

Clearly, the use of particle clouds limits the context, for even if a melt was to enter the water not as a coherent mass, but in a more-or-less broken-up state, under most conditions, additional break-up would be expected during premixing. Still, this limited context (one that may be called 'idealized premixing') is extremely attractive. The reasoning can be summarized as follows:

1. Absence of break-up allows complete characterization—a 'must' for deep understanding of the phenomena and unambiguous testing of analytical/predictive capabilities.
2. Collective-particle (cloud) behavior is of central significance, even in the presence of break-up—deep understanding of such behavior is an essential prerequisite to understanding the whole process (including break-up).
3. Deep understanding of idealized premixing can provide important insights, if not quantitative bounds (such as on the degree of voiding) on the behavior of real premixtures.
4. Finally, the approach can lead to the creation and study of liquid-particle clouds, as a means of getting to the fundamentals of propagation, i.e. the study of propagation under well-defined premixture conditions and triggers.

This line of inquiry has begun already with the MAGICO experiments (Angelini et al., 1994a), involving mostly hot particle clouds and the Berkeley Nuclear Laboratory (BNL) program (a portion actually carried out at Oxford University), involving mostly isothermal, two-dimensional clouds (a flow field as slice with thickness slightly larger than the particle diameter) (Hall and Fletcher, 1994), while related efforts have been announced (and are probably underway) also in France (Berthoud and Valette, 1994) and in Germany (Jacobs, 1994). In the same context, the MIXA experiments (Denham et al., 1992; Fletcher and Denham, 1994) in Winfrith, UK and the ALPHA experiments (Yamano et al., 1994) in JAERI, Japan, should probably also be mentioned. They both involve melts broken up into particle clouds prior to entering the water, although complete characterization of the melt particle sizes has not been made available. At the other extreme we have the more 'integral' type experiments, FARO (Magallon and Hohmann, 1994) and ALPHA being currently the more prominent, in which more-or-less coherent melt masses are let to fall into water. The present work is an outgrowth and continuation of the MAGICO experiment just mentioned. In a related effort, the PM-ALPHA code is being developed (Amarasooriya and Theofanous, 1991; Yuen and Theofanous, 1995) and we make use of it here to aid in the interpretations.

The MAGICO experiment involved liter quantities of steel particles at temperatures up to 900°C, plunging with velocities of ~ 2 m s^{-1} into saturated water pools 0.25 and 0.5 m deep. The major thrust in the new experiment is to achieve particle temperatures of up to 2000°C, hence the name, MAGICO-2000. At this temperature level radiation heat transfer becomes rather significant and leads (according to the PM-ALPHA calculations carried out in the design phase) to extensive voiding of the premixture well above the $\sim 60\%$ value reached in the original MAGICO tests. Another key objective in the design was to increase the duration of the interaction (i.e. advance from small scale to intermediate scale behavior). This was achieved by increasing the total volume of the particulate and the pool depth, which also allows much higher inlet velocities. Finally, around these two main anchors, we built an experimental program covering wide ranges of particle density, particle sizes and water subcooling. Experiments were carried out in both axisymmetric and Cartesian (2D) geometries.

Following the description of the experimental apparatus, procedures and measurement techniques (Section 2), the test program and results are given in two main parts, covering the isothermal and high temperature runs, in Section 3 and Section 4, respectively. A summary of key findings is given under concluding remarks in Section 5.

2. Experimental apparatus, procedures and measurement techniques

The principal experimental objective was to generate uniform particle clouds at temperatures approaching 2000°C. This was met by a special purpose 'furnace' designed and built in our labo-

ratory. The central element of it is a graphite block, machined into a matrix of parallel holes and slots, as illustrated in Fig. 1. The holes are to contain the particles during heating, an arrangement of miniature doors (a total of five doors, one door per row of particles) are used for this and the particles are released on command by simultaneously opening all the doors. Heating is accomplished by passing a high electrical current through the graphite 'resistor', formed by the combination of holes and slots, from one end of the block to the other. The total power available by the transformer is 12.5 kW and it is sufficient to reach the 1500–2000°C range in 7–10 h. The heating is gradual, to minimize thermal gradients/stresses and allow time for thermal equilibration between the graphite and the particulate load.

Major development work was required (for details see Angelini, 1995) to support such a 'hot' block, to build and properly operate the miniature doors, to thermally insulate the whole structure and to create the necessary inert containment for it. Both the thermal insulation barrier and the outer inert containment are provided with mechanisms to allow the particle cloud through, while

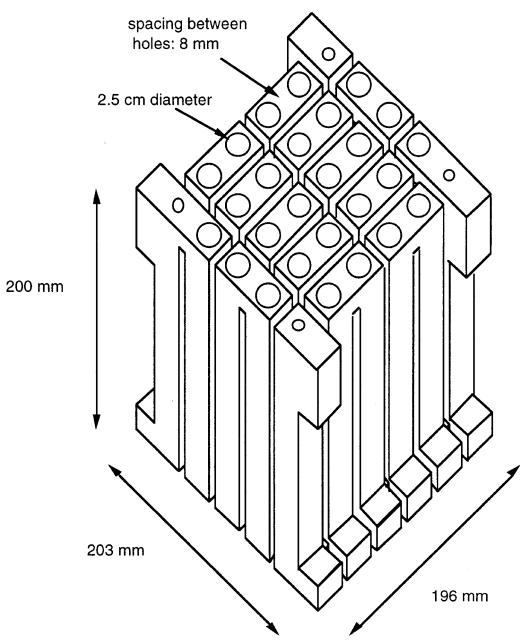

Fig. 1. Heating element in MAGICO-2000.

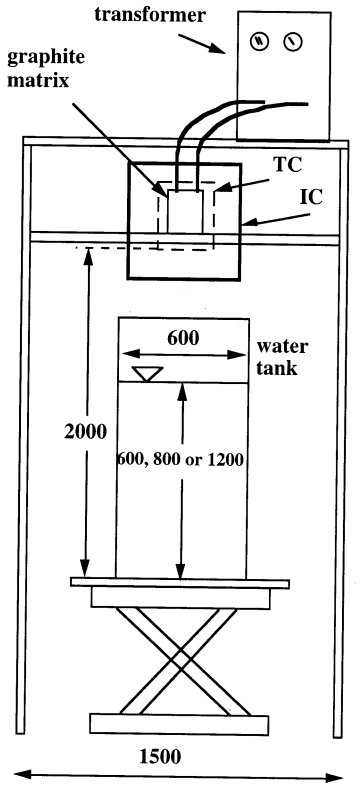

Fig. 2. Schematic of MAGICO-2000. All dimensions are in mm. TC, thermal containment; IC, inert containment.

still protecting the hot graphite block from atmospheric air and from the steam generated when the particles plunge into the water pool beneath. The overall arrangement is illustrated schematically in Fig. 2.

The various particulate materials utilized in the experiments, respective densities, sizes and shapes are listed in Table 1. Table 1 also shows the melting points and maximum temperatures attained so far with each one of them. At still higher temperatures the particles tend to 'stick' to each other in such a manner as to prevent the full and reproducible release needed to form a uniform cloud. Recently, we have developed techniques that inhibit these surface interactions and thus allow us to achieve temperatures of ~ 2000°C.

Experiments were conducted in two series. One, addressing momentum interactions, involved isothermal (room temperature) pours—the 'cold'

Table 1
Materials utilized in this study and their key characteristics

Material	Shape	Dimensions (mm)	Density (g cm^{-3})	Melting point (°C)	Maximum temperature (°C)
ZrO_2	Spherical[a]	2.4–3.4	5.5	2600	1500
ZrO_2	Spherical	6.3	5.5	2600	1500
Al_2O_3	Spherical	1.5–2.5	3.5	1950	900
SiC	Rough chips[b]	1.0–4.0	3.1	2200[c]	1200
Steel	Spherical	2.4	7.9	1400	1000

[a] Slightly off-spherical.
[b] Typical chip has dimensions $1.5 \times 2 \times 3$ mm.
[c] Dissociation point for SiC.

runs. The other included phase change effects and was carried out with high temperature pours—the 'hot' runs. Experimental conditions are summarized in Tables 2 and 3 for the 'cold' and 'hot' runs, respectively. In addition, we have carried out cold single-particle runs (they are not included in Table 2) for the purpose of testing experimental techniques and PM-ALPHA in the 'dilute' particle limit, under conditions for which an analytical comparison is possible. These runs will be referred to by the particle size and the material used.

In loading the particles into the graphite block we found a packing fraction of $\sim 60\%$. From the overall geometry (fraction of hole area to the total), we can compute that an ideal, frictionless, pour should produce a cloud of dimension similar to the graphite block with a particle volume fraction of $\sim 26\%$. Accelerating under freefall this cloud would arrive at the pool surface (normally ~ 1.4 m below) with a velocity of 5 m s^{-1}. The freefall was confirmed from the experiments; the cloud, however, was found to be considerably elongated (see Tables 2 and 3) as compared to the ideal height of 20 cm (the height of the holes). Moreover, the elongation was significantly greater in the hot runs as compared to that in the cold runs. Since frictional resistances, between the particles and graphite wall, are responsible for this elongation, the above trends indicate that the high temperatures aggravate this friction. Alternatively, it may be that this frictional limitation is aggravated by the same surface interactions that yield at higher temperatures the particle 'sticking' mentioned above and is responsible for introducing a 'delay' in the flow of each particle once the support has been removed. More work is being done to better map the particle volume fraction within the cloud, but for the time being from the dimensions of the cloud prior to impact we can find a value of average particle volume fraction and this is given for each run in Tables 2 and 3. A ZrO_2 particle cloud pouring at 1500°C is shown in Fig. 3.

Even though both the graphite matrix and the water tank have a square cross-section this geometry is referred to as 'axisymmetric'. This is to indicate our view of it as approximately axisymmetric, since via slight redistribution during the freefall the cloud cannot really be distinguished from a cylindrically shaped one (also note in Fig. 1 that with the four corner holes missing, the equivalent cross section is already quite round) and more importantly, its interaction with the water is 'all around' (largely axisymmetric).

This is to be distinguished from the 'Cartesian' geometry tank in which the width in one direction is reduced to be approximately equal to that of the pour, forcing the interaction with water to be two-dimensional on a 'plane'. The main reason for this second geometry, which was employed only for some of the cold runs, was to be able to see clearly 'behind' the mixing region after the tail end of the cloud had entered the water. In addition, it was interesting to distinguish experimentally this effect of geometry; we would expect the 2D cloud to penetrate more slowly than the axisymmetric one and provide another test point for computer codes. The designations 'AX' and 'CR' are used to denote the cold runs for the axisymmetric and Cartesian geometries, respectively.

Table 2
Specification of the cold runs

Run	Particulate	Size range (mm)	Total mass (kg)	Plunging velocity (m s^{-1})	Inlet volume fraction (%)	Cloud length/diameter (cm)[a]	Pool geometry/depth (cm)
MA.AX	Al_2O_3	1.5–2.5	5.4	5.0	9.4	43/22.0	60 × 60/60
MA.CR	Al_2O_3	1.5–2.5	5.4	5.0	9.4	43/22.0	60 × 30/60
MZ.AX	ZrO_2	2.4–3.4	8.6	5.0	10.9	37/22.0	60 × 60/60
MZ.CR	ZrO_2	2.4–3.4	8.6	5.0	10.9	37/22.0	60 × 30/60
MZD.AX	ZrO_2	2.4–3.4	8.6	4.0	10.9	37/22.0	60 × 60/120
MF.AX	Steel	2.4	12.2	5.0	13.3	37/20.0	60 × 60/60
MF.CR	Steel	2.4	12.2	5.0	13.3	37/20.0	60 × 30/60

[a] Equivalent diameter.

Table 3
Specification of the hot runs

Run	Particulate/size range (mm)	Total mass (kg)	Pour equivalent diameter (cm)	Pour duration (s)	Plunging velocity (m s^{-1})	Inlet volume fraction (%)	Particle temperature range (°C)	Water subcooling/depth (°C cm^{-1})
Z1500/0-1	ZrO_2/2.4–3.4	6.2	22.5	0.33	5.0	1.71	1300–1450	0/60
Z1500/0-2	ZrO_2/2.4–3.4	6.2	22.5	0.33	4.8	1.71	1300–1450	0/80
Z1500/3-4	ZrO_2/2.4–3.4	8.0	22.5	0.33	4.8	2.21	1300–1450	3/80
Z1500/18-5	ZrO_2/2.4–3.4	8.6	22.5	0.33	4.8	2.38	1300–1450	18/80
S1200/0-6	SiC/1.0–4.0	2.85	22.0	0.33	4.8	1.46	1150–1200	0/80

The interactions were recorded on video at the rate of 30 frames s^{-1} and at selected instances by X-ray radiographs. The video records were scanned and made available as electronic files into the computer for further processing. From these we could easily extract histories of the interaction penetration front, evolution of the interaction zone shape, rise of water (surrounding the interaction zone) level and heights of the two-phase spray ('dome') forming above the interaction in the hot runs. Both local (covering the water tank) and global (including the elevation of cloud formation immediately below the furnace) videos

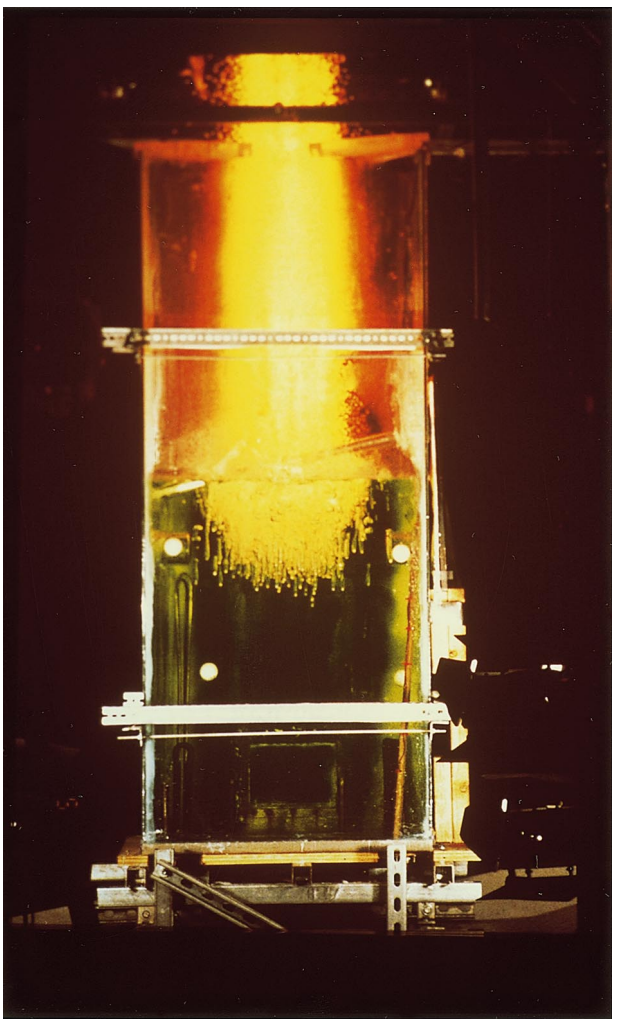

Fig. 3. Zirconium oxide pour at 1500°C.

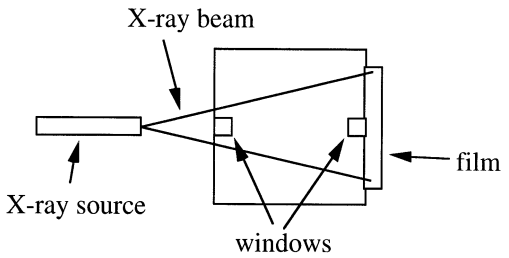

Fig. 4. Top view of X-ray arrangement in hot runs.

using Sony Hi8 camcorders were obtained. The flash X-rays were generated by a Hewlett Packard model 43734 generator equipped with a soft X-ray tube with variable energy capability of up to 360 kV. We optimized the energy level and position of the tube relative to the film (Fig. 4) for the purposes of each type of run. For the cold runs our interest was to be able to delineate any regions of high particle concentration, created through the interaction of the high-velocity cloud with the water. Such regions were predicted by the numerical simulations (PM-ALPHA), but could not be detected in the video records. The other interest of this part of the investigation was in exploring the possible existence of a 'hole' predicted to form immediately behind the submerged particle cloud and an interesting dynamic of 'closing in' a short time later. To maximize clarity, these runs were conducted in what we referred to as the Cartesian geometry.

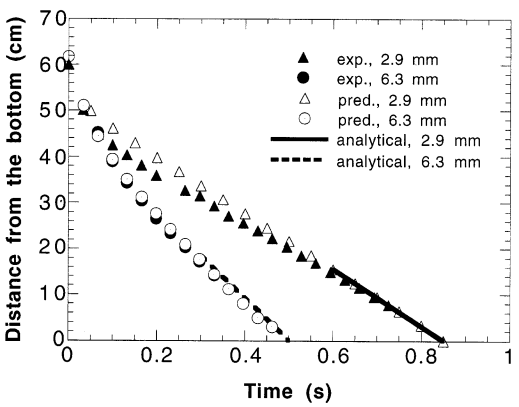

Fig. 5. Advancement of single particles, ZrO_2.

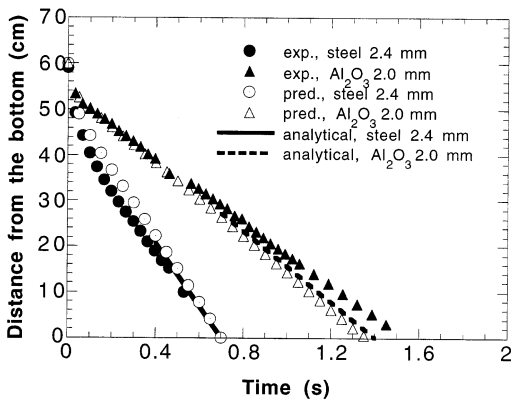

Fig. 6. Advancement of single particles, steel and Al_2O_3.

For the hot runs, our major interest was to measure the void fractions within the interaction zone. Fortunately, this became possible because, as discussed above, the particle volume fractions obtained in the hot runs were sufficiently low to allow, in between the particles, regions providing sight lines from the X-ray source to the film, involving only steam or water. The average void fraction along such lines (regions) could be measured using calibrations, obtained in situ, with known quantities of void. The approach is similar to that developed in the original MAGICO experiment (Theofanous, 1993). To further optimize discrimination here, without significantly affecting the geometry, we make use of the two 'windows' shown in Fig. 4. They are simply empty beakers, 7.5 cm in diameter and 7.5 cm long, used to remove a total of 15 cm of water from the X-ray path, thus enhancing the sensitivity of the measurement. The uncertainties in this measurement will be discussed together with the presentation of results. The same applies for the uncertainties in the measurement of the rise of the water level and of the heights of the two-phase spray. The advancements of the fronts in the pool involve determination of position and time and they are made with an accuracy of ± 3 cm and ± 0.015 s, respectively. These are small, for our purposes and they are reflected in the size of the symbols used in the figures.

Temperatures were measured continuously during heatup, using both K- and C-type thermocouples, positioned at various locations within the particulate and the graphite matrix. The maximum temperature difference is shown in Table 3 and it is indicative of the uncertainty in initial cloud temperature.

Code predictions will be shown alongside the presentation of the experimental results. The code is the version documented by Angelini et al. (1994b) and the inputs for each run are according to the specifications given in Tables 1–3. Only the following additional clarifications are necessary:

1. The axisymmetric geometry was modeled by matching the cross-sectional area of the tank. The pour area was modeled by matching, to the closest integer number of computational cells (of size 3×3 cm), the cross-sectional area of the experimental pour as obtained from the videos prior to impact on the water (the cloud appeared to expand slightly during the freefall); this involved a difference between actual pour and simulated pour of about 16% for the cold runs and 12% for the hot runs. Accordingly, the particle volume fraction has been adjusted from the average value listed in Tables 2 and 3 in order to conserve the total particle mass; sensitivity studies showed little or no effect due to this small change in particle volume fraction.
2. Calculations in the dilute limit, for comparison with the single-particle runs, were carried out by releasing a 'mini-cloud' (a packet of particles covering just one computational cell) with a particle volume fraction of 1%. That the single-particle behavior was approached was confirmed with calculations using 0.5 and 0.1% particle volume fractions that yielded the same results.
3. To determine more precisely the position of the fronts in the Eulerian calculation, we superposed Lagrangian tracer particles, made to move with the local (cell) velocity of the particulate field.
4. For the hot runs, the code calculations were carried out with a particle temperature at the middle of the range shown in Table 3. The results were not sensitive to any specification within the respective ranges.

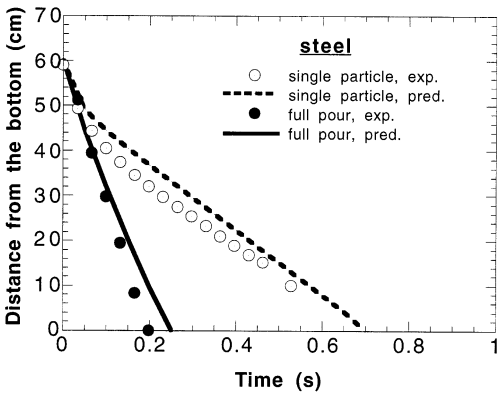

Fig. 7. Comparison between full pour (MF.AX) and single particle, steel.

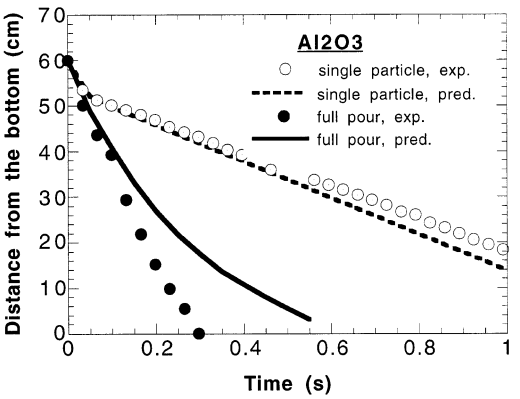

Fig. 9. Comparison between full pour (MA.AX) and single particle, Al_2O_3.

3. Results from the cold runs

All the front-propagation results from the axisymmetric cold runs are summarized in Figs. 5–10. Figs. 5 and 6 refer to single-particle runs and calculations and they include the analytically determined terminal velocities (sphere in Newton regime, constant drag coefficient $C_D = 0.44$). These comparisons are indicative of the accuracy of the experimental and data reduction procedures and the appropriateness of the analytical approach. The small deviation in terminal velocities seen for Al_2O_3 may be due to micro-bubbles trapped on the surface of the highly porous particle—such an effect appearing more pronounced given the low density of Al_2O_3. Figs. 7–9 show the collective particle effect in producing a faster-penetrating front and the influence of the particle density on this phenomenon. The faster-penetrating front is the result of the prolonged inflow of particles into the mixing region which causes an overall alteration of the velocity fields. This will be discussed more in detail later. There is some discrepancy between experiment and calculation and this appears to increase as the particulate density decreases. From the visual records it also appears to be associated with instabilities on the cloud front. These results are highly reproducible. Remarkably, a relatively small reduction in inlet velocity (from 5 to 4 m s^{-1}) is sufficient to suppress these instabilities, as shown in Fig. 10.

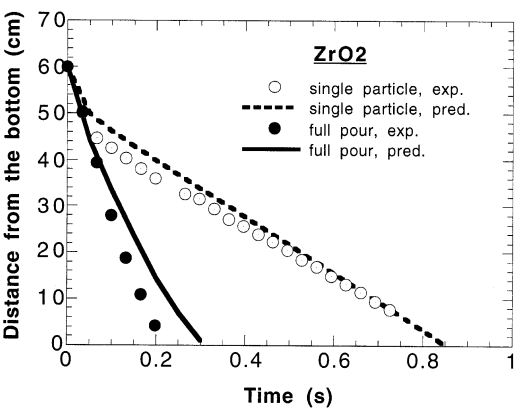

Fig. 8. Comparison between full pour (MZ.AX) and single particle, ZrO_2.

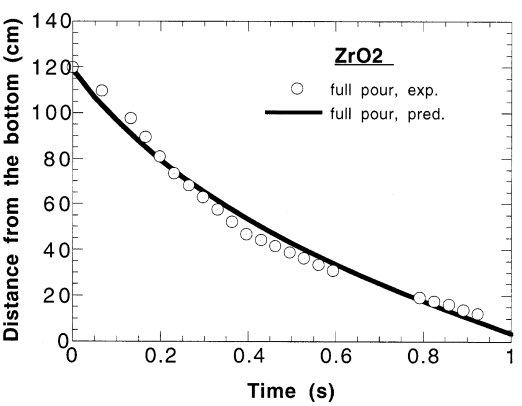

Fig. 10. Advancement of full pour of ZrO_2 particles in 1.2 m pool (MZD.AX).

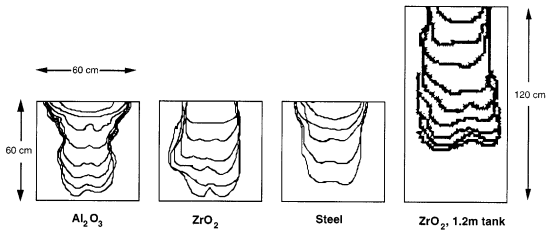

Fig. 11. Front morphologies in the cold runs in axisymmetric geometry. Contour lines are 0.033 s apart in the 60 cm runs and 0.066 s apart in the 1.2 m run.

The morphology of the front in all four cases discussed here is shown in Fig. 11. This figure, representing a two-dimensional projection of the three dimensional fronts, is not very powerful in depicting the extent of the instabilities, although it allows to discern the difference in behavior between the 'stable' steel and the 'unstable' lighter materials.

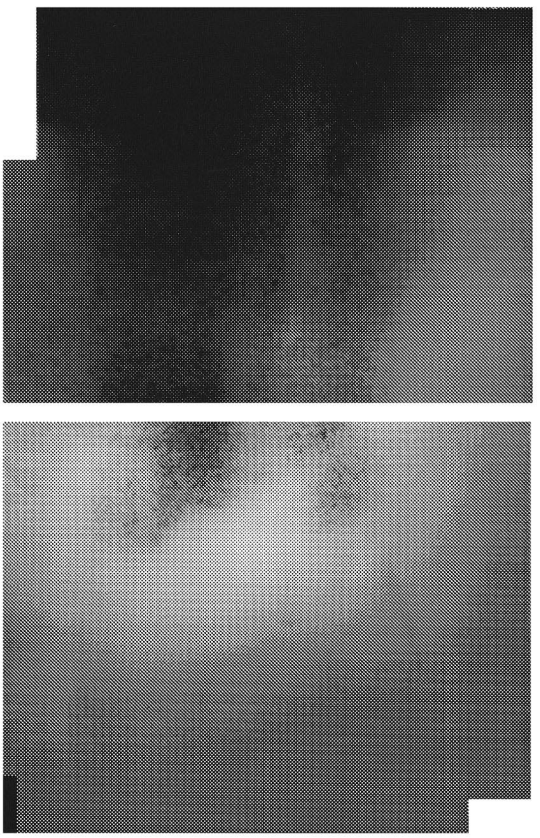

Fig. 12. Reproduction of X-ray images taken 0.15 s after impact of a pour of ZrO_2 particles on water (MZ.CR). The white area is given by the boundaries of the cassettes containing the X-ray films.

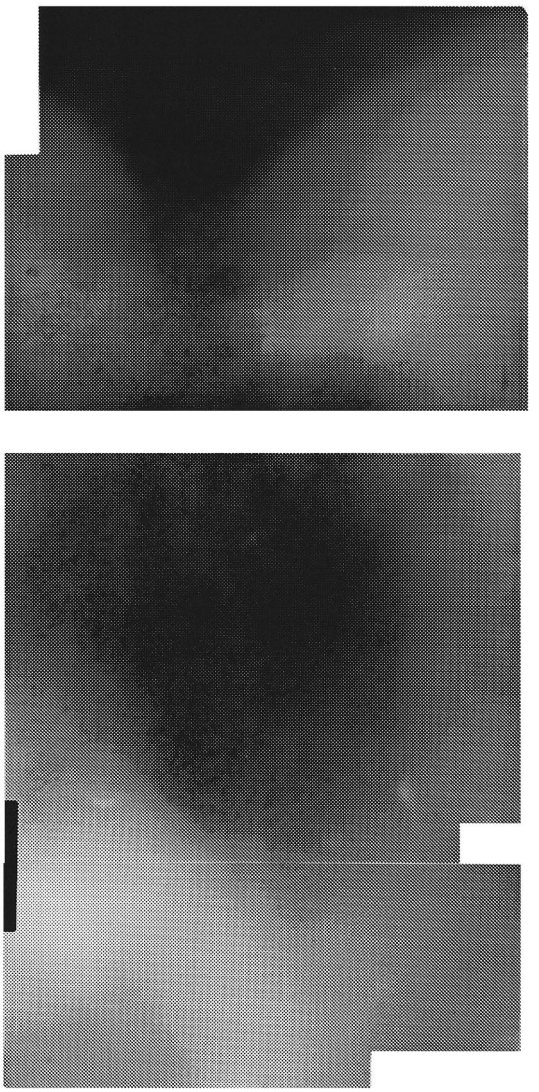

Fig. 13. Reproduction of X-ray images taken 0.25 s after impact of a pour of ZrO_2 particles on water (MZ.CR). The white area is given by the boundaries of the cassettes containing the X-ray films.

The radiographs from two Cartesian geometry runs employing a full pour of ZrO_2 particles (MZ.CR), taken at 0.15 and 0.25 s after the first contact with water, are shown in Figs. 12 and 13,

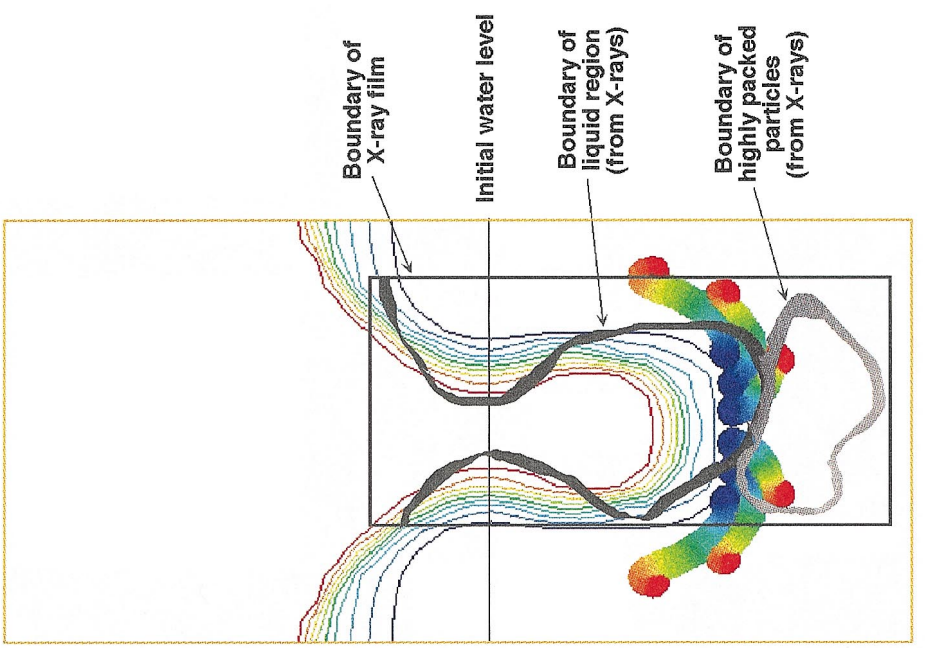

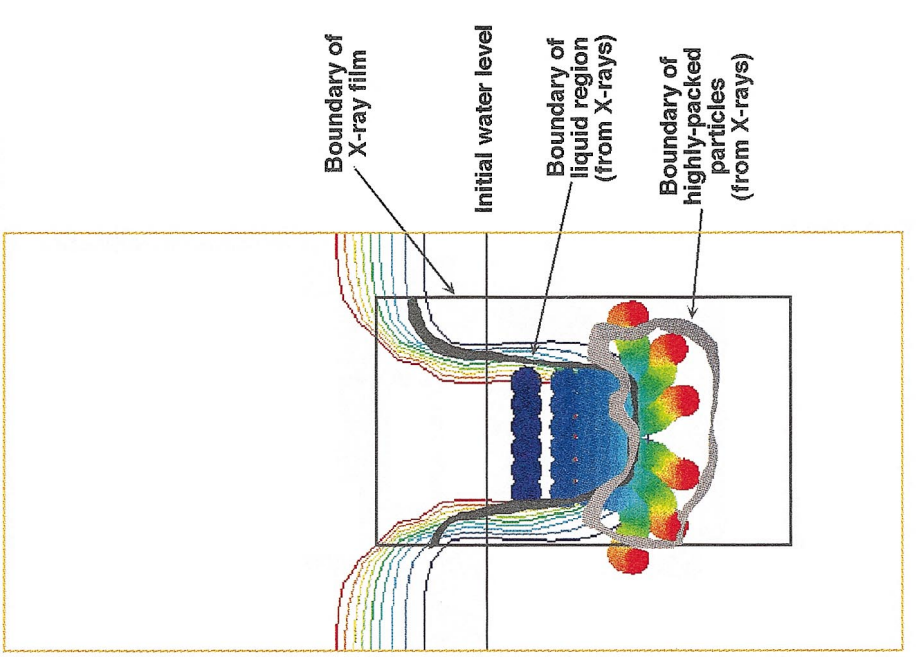

Fig. 14. Superposition of contour lines from X-ray films onto predictions from PM-ALPHA. ZrO_2 cold run (MZ.CR), 0.15 s after impact of particles on water. The prediction shows the void fraction contour lines at intervals of 10%, starting at 10%. The dots are representative of particle location (Lagrangian tracer particles). Particle volume fraction is about 18% in the zone of the red dots and about 2% in the zone of the dark blue dots.

Fig. 15. Superposition of contour lines from X-ray films onto predictions from PM-ALPHA. ZrO_2 cold run (MZ.CR), 0.25 s after impact of particles on water. The prediction shows the void fraction contour lines at intervals of 10%, starting at 10%. The dots are representative of particle location (Lagrangian tracer particles).

respectively. These figures show the formation of a 'hole-in-the-water' behind the cloud and the dense packing produced at the front. Both of these phenomena were predicted by PM-ALPHA during our work with the axisymmetric runs and motivated our investigations in the Cartesian geometry. According to our calibration, the quantity of water present in the hole region is negligible, but a few particles can be identified in it. The various regions are much more clearly identifiable in the original X-ray (than in the reproduction given here) and outlines of them are shown superposed with the PM-ALPHA results in Figs. 14 and 15. Note that the essential features, such as hole shape, including the necking-in phenomenon shown in Fig. 15 and the position of the densely packed region of particles are well-captured in the computation. Also in Fig. 15, we can see the presence of the instability that is responsible for the experimental front overtaking the calculation, as discussed already for the axisymmetric runs.

These instabilities are indeed present also in the Cartesian geometry. The behavior in this geometry is closely related to that in the axisymmetric one and this is demonstrated in Figs. 16–18, which compare directly the two behaviors. In Figs. 16 and 17 (steel and ZrO_2, respectively) the basic behavior that the planar geometry slows down the penetration is quite evident in both the experiments and the computations; the agreement with the degree of reduction is quantitative. These figures also show that the degree of discrepancy between experiments and computations due to the instabilities is quantitatively similar in the two geometries. However, in the Al_2O_3 case, Fig. 18, the instabilities overwhelm the whole behavior to such an extent that the 'constraint' of the planar two-dimensionality cannot be felt. This relates to the smaller wave length (found in this case) as compared to the depth of the flow field. The front morphologies (again projections) in the Cartesian runs are reproduced in Fig. 19.

The X-ray images are useful in explaining the above mentioned alteration of velocity fields. The continuous transfer of momentum from the particle cloud to the water results in large displacements of the water itself and the generation of a

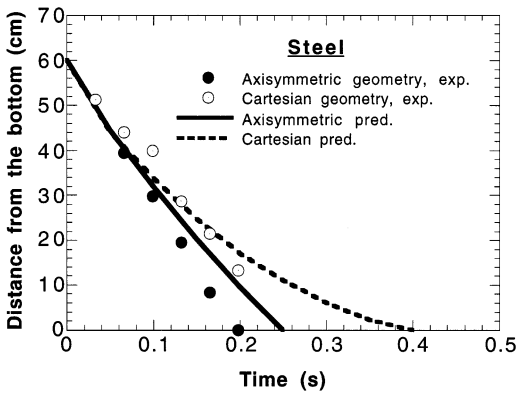

Fig. 16. Comparison between front advancements in MF.AX and MF.CR.

hole in the region behind the front. The presence of this hole implies that, aside from the first ones, the particles are falling through a gap, therefore not decelerating until they reach the front. Here their momentum is dissipated in further displacing the water ('pushing' it away) and aiding the front in its advancement, which results in being faster than that of a single particle. This behavior is quite different from that observed in a sedimenting bed: in this case, from an initial uniform suspension of particles in a liquid, gravity starts a downward motion of the particles, but the achieved terminal velocity is always lower than

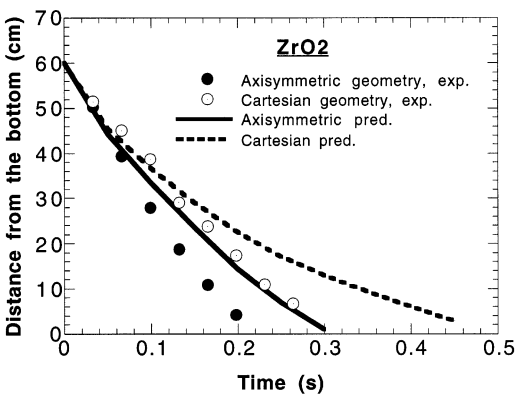

Fig. 17. Comparison between front advancements in MZ.AX and MZ.CR.

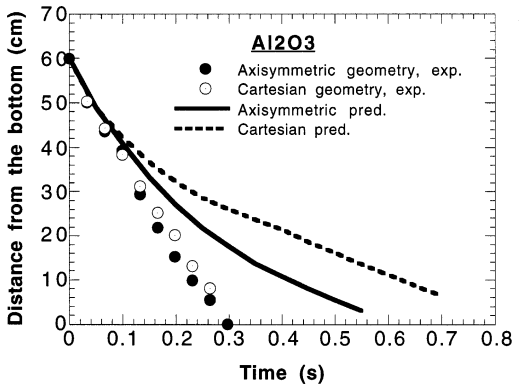

Fig. 18. Comparison between front advancements in MA.AX and MA.CR.

that for a corresponding single particle (Mirza and Richardson, 1979). This is due to the increased resistance that the liquid finds in moving upwards through the sedimenting particles in the one-dimensional geometry. It is interesting to note, however, that even in our experiments, once the inflow of particles ends, such a sedimenting behavior is asymptotically reached, as Fig. 20 clearly shows: here we compare the advancement of the particle front for runs MZ.AX (already in Fig. 8) and MZD.AX (already in Fig. 10). Initially the two cases behave very similarly, the difference in slope being due to the lower impact velocity in the 1.2 m run. However, shortly after the inflow of particle ends, the front in run MZD.AX undergoes a deceleration, with a velocity quickly approaching the terminal velocity of a corresponding single particle, represented by the continuous line (the front in run MZ.AX reaches

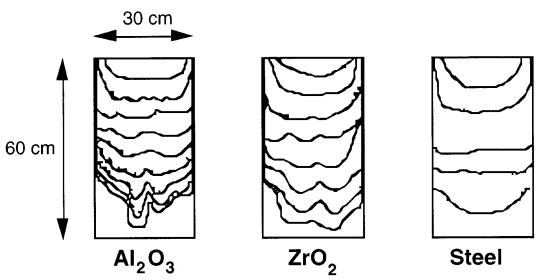

Fig. 19. Front morphologies in the cold runs in Cartesian geometry. Contour lines are 0.033 s apart.

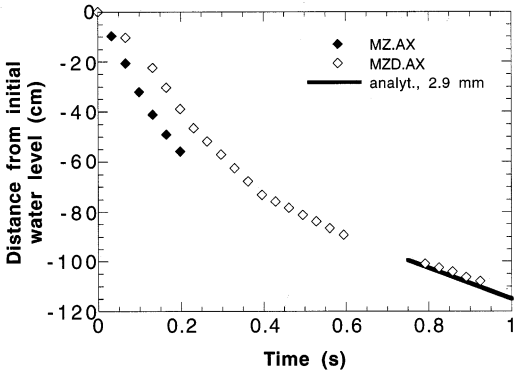

Fig. 20. Sedimenting behavior in deep pools.

the bottom before any deceleration can be detected). PM-ALPHA very effectively captures this aspect of the flow.

4. Results from the hot runs

The penetration behavior and instabilities in these runs were found to be quite similar to those observed in the cold runs. The results are summarized in Fig. 21. The behavior for run Z1500/0-2 is very similar to Z1500/0-1, which is not included in Fig. 21. We note that subcooling appears to aggravate, somewhat, the instabilities. These are responsible for the apparent disagreement in the

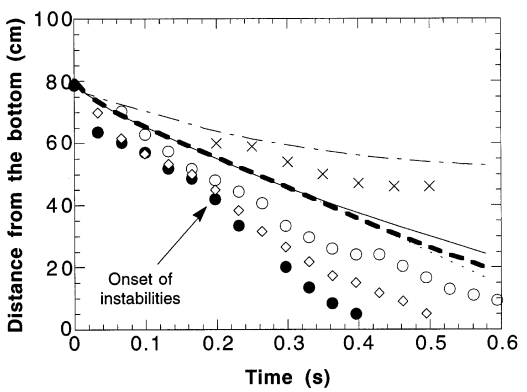

Fig. 21. Advancement of the front in hot runs. Experimental data (predictions): ○ (continuous line), Z1500/0.2; ● (dashed line), Z1500/3-4; ◇ (dotted line), Z1500/a8-5; × (dash-dot line), S1200/0-6.

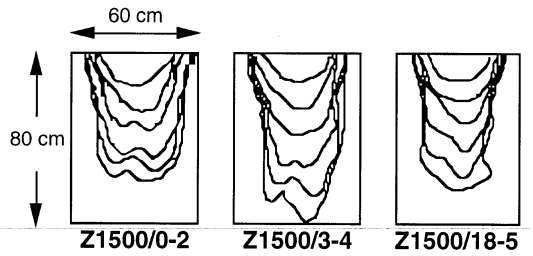

Fig. 22. Front morphologies in the hot runs. Contour lines are 0.066 s apart.

figure: 'waves' of particles stretching past the bulk of the cloud, the latter being closer to the prediction. We also note an indication of reversal in trend, compared to the cold runs: here the light cloud (SiC) is not nearly as unstable. Under strong vapor flux due to intensive boiling the light cloud decelerates rather quickly and comes almost to a halt (both in the experiment and in the calculation). The front morphologies for runs Z1500/0-2, Z1500/3-4 and Z1500/18-5 are illustrated in Fig. 22, from which one can see the different behavior of the instabilities due to subcooling.

While the instabilities express a local behavior, albeit an interesting one, of much greater significance for our purposes are the overall mixing zone development, the void fraction in it and the related flow behavior around it. In particular, the water level around it provides a measure of the overall void history as a result of phase change phenomena, while the spray dome above it provides an indication of the steaming rate resulting from the interaction. These key behaviors are presented below. Only a small sample of the results is possible within the space available; complete details have been documented and discussed by Angelini (1995).

4.1. Void fraction measurements

The measurement of void fraction is limited to the chordal average through a small region 15 cm below the initial water level. It is the only 'local' measurement among those presented here and thus strongly depends on the characteristics of the evolution of the interaction in its detail, rather than on a global behavior. As such, the measurement not only provides insight into premixing, but represents probably the most important test for computer codes.

The local void fractions found experimentally in runs Z1500/0-2 and Z1500/3-4 are compared to the predictions in Fig. 23; the experimental value has been taken 0.35 s (+ 0.05 s uncertainty) after the first impact of particles on the water. The analysis of the X-ray film is based on eight calibration films in which steps of void of known length were placed in the tank. Comparison between these films and those taken during the hot runs is facilitated by the presence of witness marks and allows us to place the uncertainty within the range shown.

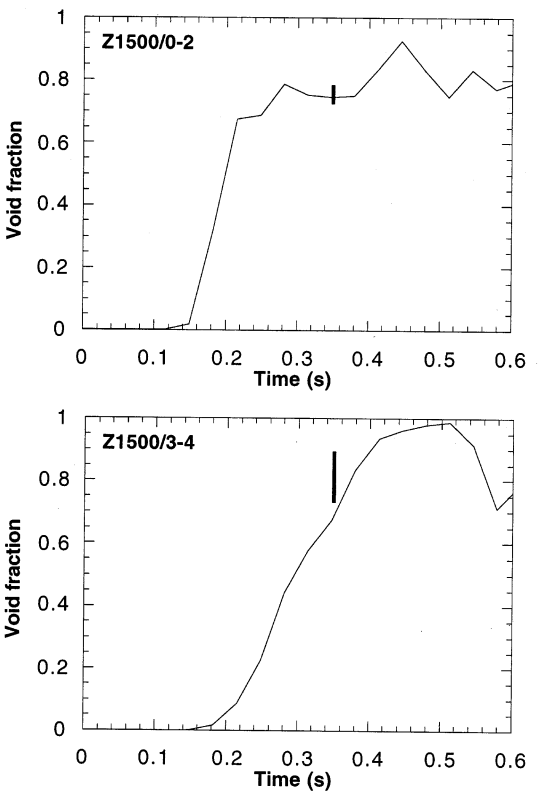

Fig. 23. Comparison between void fraction measured in runs Z1500/0-2 and Z1500/3-4 and corresponding PM-ALPHA predictions.

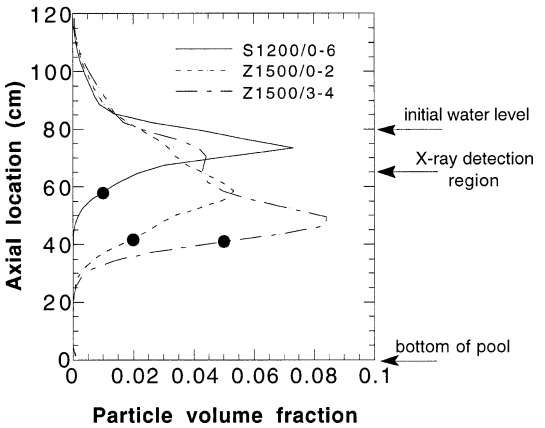

Fig. 24. Predicted particle volume fractions in hot runs at the time of X-ray trigger. ●, location of the front according to the prediction.

As expected, the prediction suggests that the effect of 3°C subcooling is to introduce a delay time in the onset of voiding. After this delay extensive voiding of the mixing region is reached, somewhat more gradually, but at even higher levels (up to 100%) than the saturated case, temporarily. This is confirmed by the experimental measurements. The highly subcooled run, Z1500/18-5, produced, in agreement with the calculation, an insignificant void (as judged by the level swell to be discussed shortly below). It was below the detection limit of the X-rays ($\sim 25\%$). In run Z1500/0-1 void fractions by X-rays were not measured.

In run Z1200/0-6 the combination of low particle density and intensive vapor generation causes the particles to undergo a strong deceleration, as already seen in Fig. 21. The ensuing particle accumulation, below and around the detection region, is responsible for essentially complete voiding of that region, and a measurement of 100% void fraction is obtained. The low particle density in this case, synergistically with the vapor production and associated momentum interaction produces quite different axial particle distributions than in the ZrO_2 runs (Fig. 24). Note in particular that in the ZrO_2 runs the X-ray is taken well behind the front and in the trailing side of the descending particle cloud (behind the concentration peak) while in the SiC run the front has just passed through this location, the particle concentration is low and on the rise as the main portion of the descending cloud is approaching. The peak in this cloud is narrower and quite high. Due to this singular behavior the comparison with the prediction is shown in Fig. 25. Note that within a few centimeters away the prediction gives a rather broad voided zone with a void fraction of $\sim 90\%$ as compared to the measured $\sim 100\%$.

By contrast, as can be seen in Fig. 26, the X-ray in run Z1500/0-2 was obtained away from the front and the associated (singular) high-sensitivity region. In run Z1500/3-4 the presence of subcooling is responsible for three distinct singular regions: the void distribution presents a maximum which is lagging the peak in the particle cloud because of the time required for the water to reach saturation first. At an even higher location, the void fraction collapses temporarily because of recirculation of subcooled water that is being displaced by the front. Incidentally, the X-ray happens to have caught the region of high void fraction.

4.2. Water level swells

The level swells for runs Z1500/0-2 and Z1500/18-5 are shown in Fig. 27. The uncertainty in measurement is in locating the somewhat disturbed (and disrupted) interface. For the calculation the upper and lower limits shown correspond

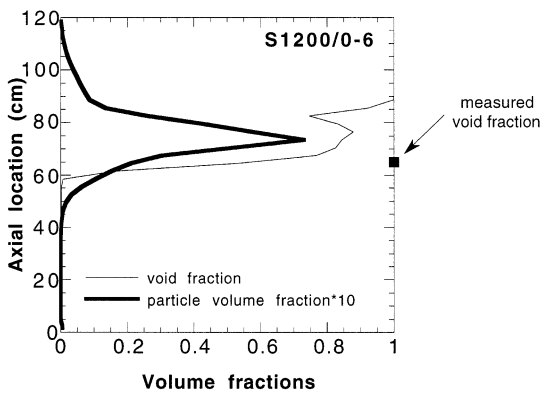

Fig. 25. Volume fraction distributions in run S1200/0-6.

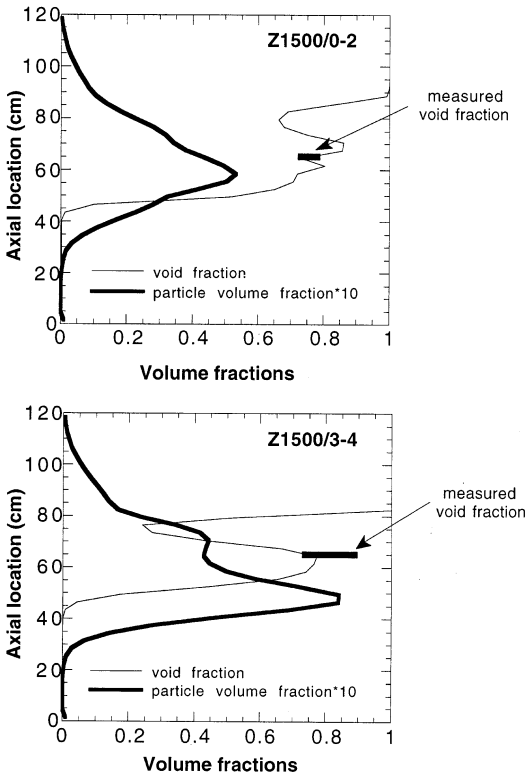

Fig. 26. Volume fraction distributions in ZrO_2 runs.

to the 50 and 90% liquid fraction contours at the interfacial region—they are indicative of the water level. The important trends in this figure are

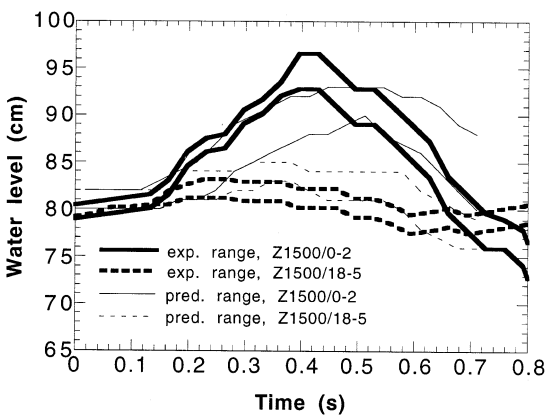

Fig. 27. Water level swells for runs Z1500/0-2 and Z1500/18-5. Predictions refer to 50 and 90% liquid contour lines.

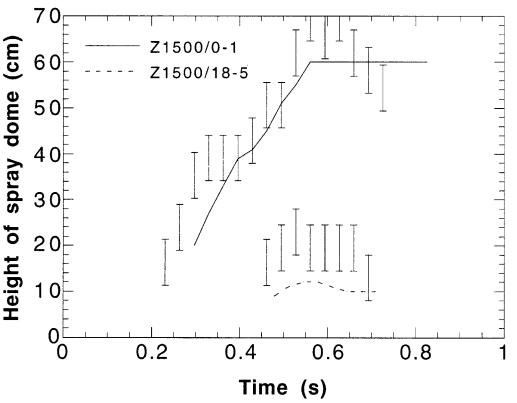

Fig. 28. Height of spray dome above initial water level for runs Z1500/0-1 and Z1500/18-5.

that 18°C subcooling suppresses voiding almost completely and that the void in the mixing zone for the saturated run peaks out and contracts. This latter effect is indicative of the flow reversal phenomenon (in the water surrounding the mixing zone) and the ETHICCA phenomenon described previously (Angelini et al., 1994b).

In run S1200/0-6 because of the shallow penetration these phenomena are less discernible, especially since the interface broke sufficiently to make measurements impossible beyond 0.3 s (the comparison up to this time with the calculation is similar to that in Fig. 27). For runs Z1500/0-1 and Z1500/3-4 the behavior is very similar to that of Z1500/0-2.

4.3. Height of spray dome

The heights of the spray dome above the initial water level for runs Z1500/0-1 and Z1500/18-5 are shown in Fig. 28. The experimental data are represented by bars which incorporate the uncertainty in their measurement and the prediction corresponds to the position of the 2% liquid volume fraction contour line (contour lines between 1 and 5% form a rather narrow band). Results similar to those of Z1500/0-1 are obtained in runs Z1500/0-2 and S 1200/0-6, while for run Z1500/3-4 these data were not available. From this figure we see that in the presence of 18°C subcooling the spray dome is almost nonexistent and forms only

after all the particles have entered the tank (~ 0.4 s), again suggesting that for this run evaporation is almost completely suppressed. The calculation predicts the same behavior. On the contrary, in saturated water large amounts of vapor are produced that escape the tank dragging liquid along with them from early in the mixing (note that the computational grid in the simulation of Z1500/0-1 is limited to 60 cm above the initial water level). It is worth pointing out the difference in scales between Figs. 27 and 28: the water level grows by a maximum of 15 cm, as opposed to 70 cm and more for the spray dome. Although both behaviors are linked to the vapor generation in the mixing region, they are completely distinguishable.

5. Concluding remarks

The MAGICO-2000 facility and the associated measurement techniques provide a unique capability to produce uniform particle clouds of temperatures up to 1500°C, currently, for the study of detailed interactions with water pools. Interesting phenomena identified under isothermal conditions are: the formation of densely packed regions at the penetrating front; the formation of a 'cavity' behind relatively dense clouds ($10 \div 14\%$ volume fraction); the development of instabilities (finger-like) at the penetrating front and; the slowing-down effect of a motion restricted to planar symmetry. Interesting phenomena quantified in hot pours include: local voiding in the mixing zone; global voiding through the level swell; the formation of a two-phase spray dome about the mixing zone and; the effects of slight (3°C) and moderate (18°C) subcooling on the above. Calculations with the PM-ALPHA code helped to interpret and probe in much greater detail than is feasible experimentally into these phenomena and showed the importance of the details for the correct simulation of the process. Only the front instability was not captured by the numerical model. All these comparisons are expected to contribute significantly to an overall scheme of code verification appropriate for the intended applications.

Acknowledgements

This work was funded by the US Department of Energy's Advanced Reactor Severe Accident Program (ARSAP) through ANL subcontract No. 23572401. We are very grateful to Tony Salmassi, who was instrumental in the design and the construction phases of the MAGICO-2000 facility. We would also like to acknowledge the contribution of Sam Ameen (Aweto Custom Printing) in the development of X-ray radiography for void fraction measurements. Steven Sorrell (DOE) and Stephen Additon (TENERA) played a key role in programmatically supporting this project.

References

Amarasooriya, W.H., Theofanous, T.G., 1991. Premixing of steam explosions: A three fluid model. Nucl. Eng. Des. 126, 23–39.

Angelini, S., 1995. The dynamics of hot particle clouds plunging into water, PhD thesis. University of California, Santa Barbara, CA.

Angelini, S., Takara, E., Yuen, W.W., Theofanous, T.G., 1994a. Multiphase transients in the premixing of steam explosions. Nucl. Eng. Des. 146, 83–95.

Angelini, S., Yuen, W.W., Theofanous, T.G., 1994b. Premixing-related behavior of steam explosions. In: Proceedings of the CSNI Specialists Meeting on Fuel-Coolant Interactions, Santa Barbara, CA, January 5–8, 1993. NUREG/CP-0127, March 1994, pp. 99–133.

Berthoud, G., Valette, M., 1994. Calculations of the premixing phase of an FCI with the TRIO MC Code. In: Proceedings of the CSNI Specialists Meeting on Fuel-Coolant Interactions, Santa Barbara, CA, January 5–8, 1993. NUREG/CP-0127, March 1994, p. 27.

Denham, M.K., Tyler, A.P., Fletcher, D.F., 1992. Experiments on the mixing of molten uranium dioxide with water and initial comparisons with CHYMES code calculations. In: Proceedings of the Fifth International Topical Meeting on Reactor Thermal Hydraulics (NURETH5), Salt Lake City, UT, September 21–24, vol. 6. p. 1667.

Fletcher, D.F., Denham, M.K., 1994. Validation of the CHYMES mixing model. In: Proceedings of the CSNI Specialists Meeting on Fuel-Coolant Interactions, Santa Barbara, CA, January 5–8, 1993. NUREG/CP-0127, March 1994, p. 89.

Hall, R.W., Fletcher, D.F., 1994. Validation of CHYMES: simulant studies. In: Proceedings of the CSNI Specialists Meeting on Fuel-Coolant Interactions, Santa Barbara, CA, January 5–8, 1993. NUREG/CP-0127, March 1994, p. 70.

Jacobs, H., 1994. Analysis of large-scale melt-water mixing events. In: Proceedings of the CSNI Specialists Meeting on Fuel-Coolant Interactions, Santa Barbara, CA, January 5–8, 1993. NUREG/CP-0127, March 1994, p. 14.

Magallon, D., Hohmann, H., 1994. High pressure corium melt quenching tests in Faro. In: Proceedings of the CSNI Specialists Meeting on Fuel-Coolant Interactions, Santa Barbara, CA, January 5–8, 1993. NUREG/CP-0127, March 1994, p. 1.

Mirza, S., Richardson, J.F., 1979. Sedimentation of suspensions of particles of two or more sizes. Chem. Eng. Sci. 34, 447–454.

Theofanous, T.G., 1993. The study of steam explosions in nuclear systems. In: International Seminar on Physics of Vapor Explosion, Tomakomai, Hokkaido, Japan, October 25–28, 1993. pp. 5–26.

Theofanous, T.G., Yuen, W.W., 1994. The prediction of dynamic loads from ex-vessel steam explosions. In: Proceedings of the International Conferance on New Trends in Nuclear System Thermohydraulics, Pisa, May 30 to June 2, 1994. pp. 257–270.

Yamano, N., Sugimoto, J., Maruyama, Y., Soda, K., 1994. Studies on fuel coolant interactions during core melt accident of nuclear power plant. In: Proceedings of the CSNI Specialists Meeting on Fuel-Coolant Interactions, Santa Barbara, CA, January 5–8, 1993, NUREG/CP-0127, March 1994, p. 271.

Yuen, W.W., Theofanous, T.G., 1995. PM-ALPHA: a Computer Code for Addressing the Premixing of Steam Explosions. DOE/ID-10502, May 1995.